

Hydrogen density-of-states distribution in β -Ga₂O₃

Cite as: J. Appl. Phys. 129, 195704 (2021); doi: 10.1063/5.0030903

Submitted: 25 September 2020 · Accepted: 30 April 2021 ·

Published Online: 18 May 2021



N. H. Nickel^{a)}  and K. Geilert

AFFILIATIONS

Helmholtz-Zentrum Berlin für Materialien und Energie GmbH, Institut für Silizium Photovoltaik, Kekuléstr. 5, 12489 Berlin, Germany

^{a)}Author to whom correspondence should be addressed: nickel@helmholtz-berlin.de

ABSTRACT

Hydrogen bonding in β -Ga₂O₃ is investigated using hydrogen effusion measurements. The samples were grown by plasma-assisted pulsed laser deposition. With increasing deposition temperature, the total H concentration decreases from 8.1×10^{19} to 9.2×10^{18} cm⁻³. The dependence of the hydrogen chemical potential, μ_{H} , on the H concentration is derived from the effusion spectra and subsequently used to determine the H density-of-states distribution. β -Ga₂O₃ deposited at $T_{\text{dep}} \leq 723$ K exhibits a needle-like peak in the H density-of-states distribution at ≈ 1.8 eV below the H transport states. With increasing T_{dep} , the H density-of-states changes and two broad peaks emerge that are located at ≈ 1.7 and 2.4 eV below the H transport states for $T_{\text{dep}} \geq 873$ K.

© 2021 Author(s). All article content, except where otherwise noted, is licensed under a Creative Commons Attribution (CC BY) license (<http://creativecommons.org/licenses/by/4.0/>). <https://doi.org/10.1063/5.0030903>

I. INTRODUCTION

For a long time, it was believed that the main property of hydrogen is its ability to passivate localized defects in semiconductors. However, extensive research carried out over the last three decades revealed a multitude of properties in a number of semiconductors such as silicon, germanium, GaAs, GaN, ZnO, GaP, and others. The properties of hydrogen comprise the compensation and neutralization of impurities and intentionally incorporated dopants, the formation of extended structural defects, and the formation of donor or acceptor states that influence the Fermi energy.^{1,2} In many wide bandgap oxides, the presence of H gives rise to n-type conductivity. For β -Ga₂O₃, this unintentional doping effect has been attributed to the presence of either interstitial (H_i) or substitutional hydrogen at an oxygen site (H_O). According to *ab initio* calculations, both centers act as shallow donors.³ This theoretical prediction was corroborated by muon spin relaxation measurements.⁴ Recently, infrared absorption measurements showed that the free-carrier absorption increases upon annealing of β -Ga₂O₃ in H₂ atmosphere. The source of the additional charge carriers was related to the formation of shallow H donor complexes.⁵

Experimental evidence for H complexes in β -Ga₂O₃ is still sparse and it is nonexistent for the theoretically predicted donor centers H_i and H_O. The most prominent hydrogen complex was identified by FT-IR measurements. This electrically neutral complex

consists of two H atoms in a Ga vacancy (V_{Ga}-2H) that is aligned along the [102] crystallographic direction.⁶ In addition to this H complex, more than ten additional vibrational modes that are related to the presence of hydrogen have been reported recently. While the microscopic origin of most of these vibrational modes are yet unknown, some were assigned to specific H complexes.^{5,7-9}

In this paper, we present comprehensive information on hydrogen binding energies in plasma-assisted pulsed laser deposited (PLD) β -Ga₂O₃. For this purpose, hydrogen and deuterium effusion measurements are performed, and from the effusion spectra, the H density-of-states (H DOS) distribution is derived, which provides detailed information on hydrogen binding energies. Samples grown at low deposition temperatures exhibit a pronounced peak in the H density-of-states located about 1.8 eV below the H transport states. At higher deposition temperatures, the H density-of-states changes and is mainly composed of two broad peaks centered at 1.7 and 2.4 eV below the H transport states. Interestingly, about 60% of the H atoms are accommodated with binding energies larger than 2 eV.

II. EXPERIMENT

The experiments shown in this publication were performed on polycrystalline β -Ga₂O₃ thin films that were grown by plasma-assisted PLD. As excitation source, a KrF excimer laser was employed that emitted ultraviolet (UV) light with a wavelength of 248 nm and a

pulse length of 25 ns. The laser was operated at a repetition rate of 10 Hz. The UV light was focused on gallium oxide targets that were fabricated from ultra-pure powder. In the first step, the targets were cold pressed with a pressure of $\approx 110 \text{ kg/cm}^2$. Subsequently, the gallium oxide targets were sintered in ambient air at a temperature of 1500°C for 5 h. Nominally, undoped $\beta\text{-Ga}_2\text{O}_3$ thin films were deposited on *c*-axis oriented sapphire substrates. The substrates were mounted upside down at a distance of 10 cm to the target. To avoid contamination of the specimens with aluminum from the substrate, a magnesium oxide (MgO) layer with a thickness of $\approx 5 \text{ nm}$ that acts as a diffusion barrier was deposited on top of the sapphire substrates. $\beta\text{-Ga}_2\text{O}_3$ samples were grown at substrate temperatures ranging from 425 to 700°C . Monatomic oxygen generated in an optically isolated remote microwave plasma was added during the growth to achieve a stoichiometric composition of the specimens. In order to investigate hydrogen bonding, the tracer element deuterium (^2H), which is readily identifiable and shows similar chemical behavior as hydrogen, was added to the microwave plasma. The deuterium and oxygen flow rates were set to 30 sccm, and the deposition pressure was kept at $p = 5.6 \times 10^{-3} \text{ mbar}$. These conditions yielded a growth rate of about $dd/dt = 4.2 \text{ \AA/s}$. The microscopic structure was investigated using scanning electron microscopy (SEM). In addition, all samples were characterized using Raman backscattering spectroscopy. For this purpose, a micro-Raman setup was used with an excitation wavelength of $\lambda = 633 \text{ nm}$. The measurements were performed at room temperature.

Insight into hydrogen bonding was obtained from hydrogen effusion measurements. Samples with a size of 0.4 cm^2 were placed in ultrahigh vacuum with a background pressure of $p \approx 6 \times 10^{-9} \text{ mbar}$. Then, the specimens were annealed with a heating rate of 20 K/min , while the molecular flux of hydrogen, deuterium, and HD was recorded using a quadrupole mass spectrometer. The relative ion current obtained from the quadrupole mass spectrometer was calibrated using the known neon flux through a capillary. Details on the analysis of the hydrogen effusion data are described in Sec. IV.

Since the properties of hydrogen and deuterium do not show significant differences regarding migration and bonding,^{10–12} the terms hydrogenation and deuteration will be used interchangeably in Secs. III–V.

III. RESULTS

Surface and cross-sectional SEM micrographs of plasma-assisted PLD grown $\beta\text{-Ga}_2\text{O}_3$ samples are shown in Fig. 1. The depicted specimens were deposited at $T_{\text{dep}} = 723$ and 973 K . The surface micrographs shown in Figs. 1(a) and 1(b) indicate that the samples are composed of small grains and, hence, are polycrystalline. In addition, with increasing deposition temperature, the surface roughness increases. The cross-sectional SEM micrographs confirm that the specimens are composed of small crystalline grains. At $T_{\text{dep}} = 723 \text{ K}$, an average grain sizes of $75\text{--}130 \text{ nm}$ is observed [Fig. 1(c)]. With increasing deposition temperature, the grain distribution becomes more inhomogeneous and at $T_{\text{dep}} = 973 \text{ K}$, small and large grains with diameters ranging from 100 to 260 nm are observed [Fig. 1(d)].

Further insight into the structural properties of the PLD grown samples was obtained from Raman backscattering measurements. $\beta\text{-Ga}_2\text{O}_3$ is a monoclinic crystal and belongs to the space

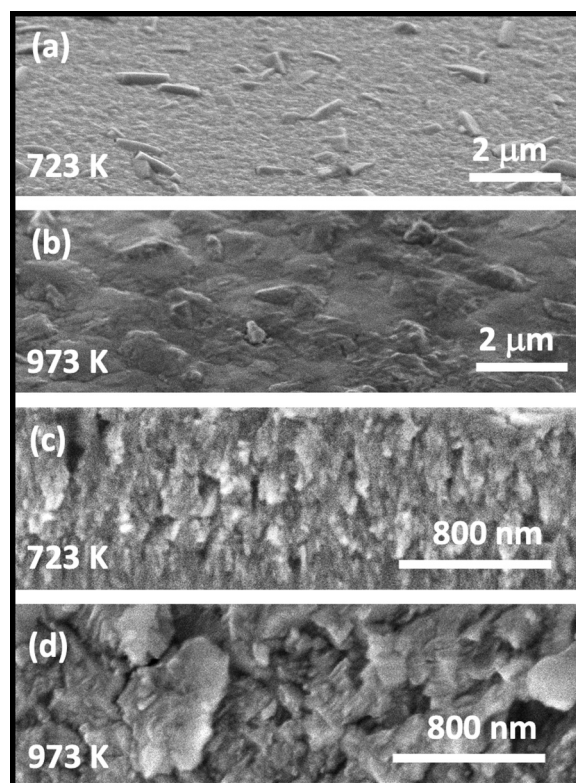


FIG. 1. SEM micrographs of PLD grown $\beta\text{-Ga}_2\text{O}_3$ thin films. The samples were deposited at $T_{\text{dep}} = 723$ and 973 K . (a) and (b) show the surface of the specimens, while cross sections are depicted in (c) and (d). The sample grown at $T_{\text{dep}} = 973 \text{ K}$ exhibits grain sizes that vary between 75 and 130 nm . At higher deposition temperatures, grain sizes of up to $\approx 260 \text{ nm}$ are observed in addition to small grains of $75\text{--}130 \text{ nm}$ diameter.

group $C_{2/m}$.¹³ The primitive unit cell contains 10 atoms resulting in 3 acoustic and 27 optical phonon modes. The zone centered phonon modes at $k = 0$ are given by¹⁴

$$\Gamma = 10A_g + 5B_g + 8B_u + 4A_u, \quad (1)$$

where A_g and B_g modes are Raman active, while A_u and B_u modes are infrared active. Raman backscattering spectra measured on the PLD grown samples are shown in Fig. 2. In the wavenumber range from 100 to 500 cm^{-1} , up to seven phonon modes are observed. Even at the lowest deposition temperature, six prominent phonon modes, $A_g^{(1)}$, $A_g^{(2)}$, $A_g^{(3)}$, $A_g^{(5)}$, $A_g^{(7)}$, and $B_g^{(2)}$, are observed. It is interesting to note that the broadest phonon mode, $A_g^{(7)}$, has a linewidth of $\Gamma = 16.9 \text{ cm}^{-1}$, while the narrowest linewidth of $\Gamma = 2.8 \text{ cm}^{-1}$ was measured for the $A_g^{(2)}$ mode. The vibrational frequencies of the phonon modes and their linewidths are summarized in Table I. For comparison, the phonon modes of undoped single crystal $\beta\text{-Ga}_2\text{O}_3$ were measured [see the blue dashed curve in Fig. 2(f)]. The spectral locations and linewidths of the phonon modes of PLD grown $\beta\text{-Ga}_2\text{O}_3$ are in good agreement to those measured on single crystal

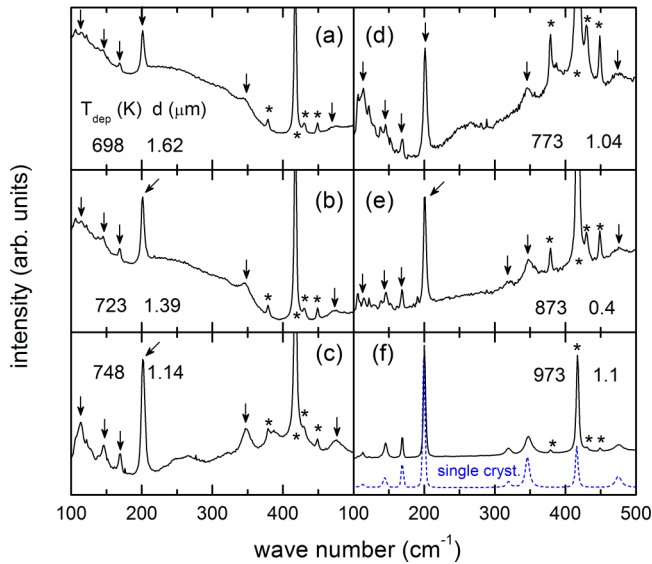


FIG. 2. Raman backscattering spectra of PLD grown β -Ga₂O₃ thin films. The samples were irradiated with the 633 nm line of a HeNe laser. The deposition temperature, T_{dep} , and sample thickness, d , are indicated in the figure. The fundamental phonon modes, $A_g^{(1)}$ to $A_g^{(7)}$ and $B_g^{(2)}$, are indicated by arrows, and the corresponding frequencies are summarized in Table I. Phonon modes that originate from the sapphire substrates are marked with an asterisk. The blue dashed line in (f) shows the phonon modes of undoped single crystal β -Ga₂O₃. All spectra are normalized to unity at the $A_g^{(3)}$ mode.

β -Ga₂O₃. This is a strong indication that the PLD grown specimens are polycrystalline and do not contain an amorphous phase. During the PLD growth of β -Ga₂O₃ residual, water vapor dissociates in the plasma into OH and H upon electron impact,^{15,16} which leads to the incorporation H atoms.¹⁷ This is advantageous for hydrogen effusion measurements. Since hydrogen migration is governed by monatomic diffusion,¹⁷ HD molecules can form at the surface of the sample before they are abstracted into the vacuum of the effusion setup. At low hydrogen or deuterium concentrations,

the presence of both isotopes in the specimens improves the sensitivity of the measurement due to the formation of HD molecules.

Specimens deposited up to $T_{\text{dep}} = 748$ K showed a H₂, D₂, and an HD signal in the effusion measurements with an identical temperature dependence. However, with increasing deposition temperature, T_{dep} , the deuterium concentration in the samples decreases. Since H and D migrate as atoms in β -Ga₂O₃,¹⁷ the likelihood that two D atoms recombine at the sample surface and form D₂ molecules decreases, which results in a decrease of the D₂ flux. However, at low D concentrations, most deuterium atoms are in close proximity of an H atom at the surface and hence form HD molecules. Therefore, to render the effusion data comparable for all samples, the molecular HD flux, dN_{HD}/dt , is shown as a function of the annealing temperature, T , in Fig. 3.

Significant out-diffusion of HD is observed at temperatures exceeding 500 K. The onset of the effusion curves is similar for all samples. However, β -Ga₂O₃ samples deposited at $T_{\text{dep}} = 698$ and 723 K reveal a pronounced peak in the HD effusion rate at $T = 736$ and 731 K, respectively. As the deposition temperature increases, the magnitude of the peak decreases, which is accompanied by a broadening of the peak. In addition, the position of the effusion peak shifts to lower temperatures [Figs. 3(a) and 3(b)]. Previously, a similar but less pronounced peak was observed at a temperature of about 850 K.¹⁷ Although the growth parameters were the same as for the specimens investigated in this work, they did not contain a diffusion barrier for aluminum from the sapphire substrate. Hence, it is likely that the observation of the main effusion peak at 850 K (Ref. 17) originates from an interaction of hydrogen with Al impurities.

For specimens deposited at $T_{\text{dep}} = 748$ K, the prominent peak shown in Figs. 3(a) and 3(b) disappears and two new broad peaks centered at $T = 623$ and 882 K develop [Fig. 3(c)]. With increasing T_{dep} , the broad peaks shift to higher temperatures: for β -Ga₂O₃, deposited at $T_{\text{dep}} = 773$ K, the peaks reside at $T = 633$ and 885 K. Eventually, with a further increase of T_{dep} , only the low temperature peak is clearly observable at $T = 643$ and 655 K for $T_{\text{dep}} = 873$ and 973 K, respectively. For these specimens, the effusion spectra show a nearly constant value at $T > 800$ K.

The total H concentration, C_{H} , of the β -Ga₂O₃ samples was derived by integrating the effusion data shown in Fig. 3 according to

TABLE I. Phonon modes and their spectral positions, ω , and linewidths, Γ , of β -Ga₂O₃, given in cm⁻¹. The samples were grown by pulsed laser deposition at different substrate temperatures, T_{dep} , and showed a polycrystalline nature.

Phonon mode	T_{dep} (K)											
	698		723		748		773		873		973	
	ω	Γ	ω	Γ	ω	Γ	ω	Γ	ω	Γ	ω	Γ
$A_g^{(1)}$	113	3.6	113	4.3	113	10	114	4.0	114	4.7	113	5.9
$B_g^{(2)}$	145	4.5	145	7.6	146	6.3	145	3.6	146	4.0	145	5.9
$A_g^{(2)}$	168	3.7	168	3.7	169	4.3	168	3.9	168	2.8	169	3.1
$A_g^{(3)}$	201	5.6	201	5.7	201	6.2	201	5.8	201	4.7	200	3.9
$A_g^{(4)}$	320	10.2	320	8.4
$A_g^{(5)}$	346	12.9	347	15.7	347	13.2	346	12.4	347	14.2	347	12.3
$A_g^{(7)}$	473	12.2	473	13.6	474	14.4	476	13.9	476	16.9	476	14.0

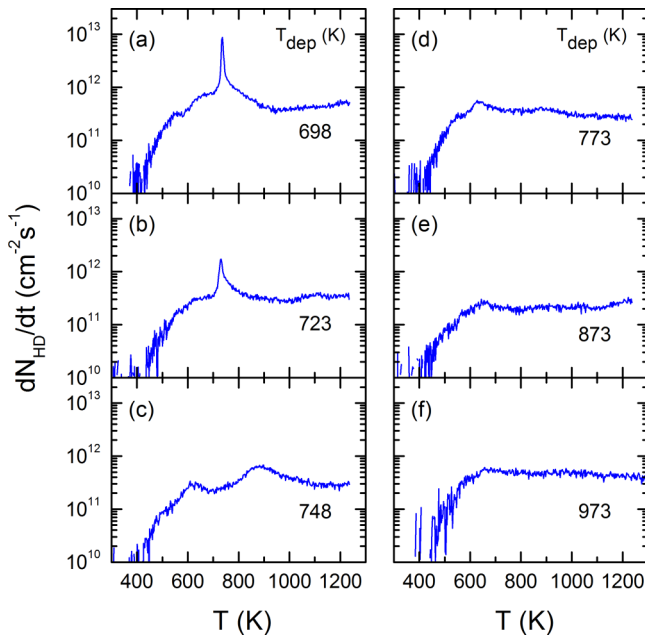


FIG. 3. Effusion rate of HD molecules, dN_{HD}/dt , as a function of the annealing temperature, T . The β -Ga₂O₃ specimens were grown at different deposition temperatures ranging from $T_{dep} = 698$ – 973 K using plasma-assisted PLD. The measurements were performed with a heating rate of 20 K/min.

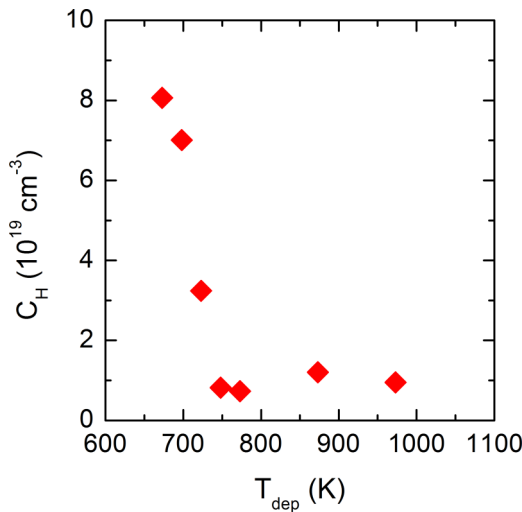


FIG. 4. Hydrogen concentration, C_H , of β -Ga₂O₃ as a function of the deposition temperature, T_{dep} . The data were obtained by integration of the effusion curves, taking into account the heating rate and the sample thickness. For specimens grown at $T_{dep} < 748$ K, the total H concentration is given by the sum of the HD, H₂, and D₂ concentrations.

$$C_H = \frac{2}{r_H d} \int \frac{dN_H}{dt} dT, \quad (2)$$

where r_h is the heating rate and d is the sample thickness.

For specimens deposited at temperatures up to $T_{dep} = 748$ K, C_H also contains the contribution of the hydrogen and the deuterium flux; for samples deposited at higher temperatures, contributions of H₂ and D₂ are neglectable. In Fig. 4, C_H is shown as a function of the deposition temperature. The highest hydrogen concentration of $C_H = 8.1 \times 10^{19} \text{ cm}^{-3}$ is observed in specimens deposited at 698 K. With increasing T_{dep} , the hydrogen concentration decreases and approaches an average value of $C_H \approx 9.2 \times 10^{18} \text{ cm}^{-3}$ for $T_{dep} > 748$ K. The constant H concentration at higher deposition temperatures indicates that plasma-assisted PLD changes the growth parameters of β -Ga₂O₃ from thermal equilibrium conditions, which results in the incorporation of more H atoms at higher deposition temperatures as one would expect from the fact that the H chemical potential moves away from the H transport energy with increasing temperature.

IV. DISCUSSION

In correspondence to the electronic density-of-states, a similar description can be used for hydrogen in a semiconductor. The electronic density-of-states provides the number of states per unit volume at a given energy level that can be occupied with electrons. It is a characteristic quantity that directly connects to the band structure of a solid. More importantly, without external influence such as doping or alloying the electronic density-of-states does not change and reflects a key property of a solid. A similar description can be made for hydrogen where the density-of-states depicts the number of H atoms accommodated at a given energy. However, the H density-of-states is not a static quantity since H has the ability to generate sites in a lattice by breaking chemical bonds, passivating defect states, and neutralizing dopants.^{1,2}

From hydrogen effusion data, the H density-of-states can be deduced. For this purpose, it is necessary to establish the relationship between the hydrogen concentration and the H chemical potential. The position of the H chemical potential with respect to the migration saddle point for H diffusion, $E_M - \mu_H$, can be derived from the hydrogen effusion rate,¹⁸

$$\frac{dN_H}{dt} = N_H^0 \exp\left(-\frac{E_M - \mu_H}{kT}\right), \quad (3)$$

where N_H^0 is the flux prefactor and k is Boltzmann's constant. The prefactor is given by $N_H^0 \approx 2\nu a D_S/d$, where ν is the attempt frequency, a is the mean free path, and D_S is the density of surface states. With a typical attempt frequency of $\approx 10^{13}$ Hz, a mean free path for H migration of 2.9 Å and a concentration of surface states of $\approx 10^{15} \text{ cm}^{-2}$, the prefactor can be estimated to $d \times N_H^0 \approx 1.72 \times 10^{21} \text{ s}^{-1} \text{ cm}^{-1}$. When calculating the H chemical potential using Eq. (2), the prefactor N_H^0 is in the argument of the logarithm. Therefore, even an error of one order of magnitude for the prefactor results in an error of only 100 meV for the position of the H chemical potential.

In Fig. 5, the position of the H chemical potential with respect to the H migration saddle point, $E_M - \mu_H$, is shown as a function of the hydrogen concentration, C_H . At high H concentrations, the chemical potential resides at $E_M - \mu_H \approx 0.9$ eV independent of the deposition temperature and decreases rapidly to $E_M - \mu_H \approx 1.5$ eV while C_H remains constant. Specimens that are grown at $T_{\text{dep}} \leq 723$ K exhibit a constant chemical potential at $E_M - \mu_H \approx 1.88$ eV for H concentrations between $C_H = 7.4 \times 10^{18}$ and 1.4×10^{19} cm⁻³. The effect is more pronounced for samples deposited at lower temperatures [Fig. 5(a)]. Commonly, pinning of the H chemical potential occurs when μ_H resides in a large density-of-states. Interestingly, pinning of μ_H is observed only in β -Ga₂O₃ grown at low deposition temperatures. As T_{dep} increases, pinning of the H chemical potential becomes less pronounced and disappears for specimens grown at $T_{\text{dep}} \geq 748$ K. With decreasing H concentration, μ_H moves away from the migration saddle point and approaches a value of $E_M - \mu_H \approx 3.2$ eV at $N_H = 1 \times 10^{18}$ cm⁻³.

The hydrogen concentration is given by the following equation:

$$C_H = \int_{-\infty}^{\infty} D_H(E) f(T, E, \mu_H) dE, \quad (4)$$

where D_H is the hydrogen density-of-state distribution, E is the H binding energy, T is the temperature, and $f(T, E, \mu_H)$ is the occupation

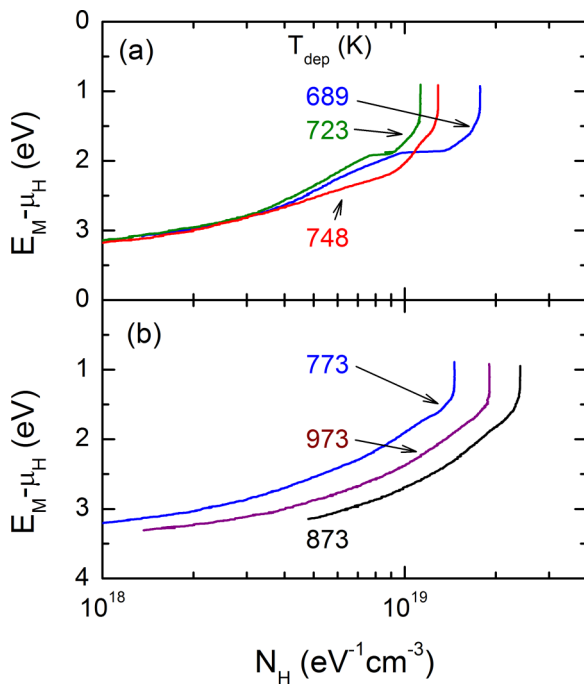


FIG. 5. Dependence of the hydrogen chemical potential, $E_M - \mu_H$, on the H concentration in β -Ga₂O₃ thin films that were grown at different deposition temperatures, T_{dep} . The H chemical potential is shown in relation to the H migration saddle point, E_M . The data were derived from the effusion spectra plotted in Fig. 3.

function. Since the partial differentiation of the occupation function yields its maximum value for $E = \mu_H$, the hydrogen density-of-states can be derived using the relation,¹⁸

$$D_H(\mu_H) \approx \frac{\partial C_H}{\partial \mu_H}. \quad (5)$$

The hydrogen density-of-states distributions obtained for plasma-assisted PLD grown β -Ga₂O₃ samples are plotted in Fig. 6. The most striking sets of data are obtained on specimens grown at $T_{\text{dep}} = 698$ and 723 K that exhibit a needle-like peak in the H density-of-states distribution at $E_M - \mu_H = 1.74$ and 1.81 eV, respectively [Figs. 6(a) and 6(b)]. In addition, both curves exhibit a shoulder in the H DOS located at $E_M - \mu_H = 1.8$ and 1.86 eV. The increase of the deposition temperature by only 25 K resulted in a shift of the peaks in the H density-of-states to larger energies. In addition, the β -Ga₂O₃ sample grown at 723 K exhibits two less pronounced peaks centered at $E_M - \mu_H \approx 1.67$ and ≈ 2.8 eV. As the deposition temperature increases further, the H density-of-states distribution undergoes a pronounced change. Samples grown at $T_{\text{dep}} = 748$ K exhibit two distinctive peaks centered at $E_M - \mu_H = 1.57$ and 2.0 eV [Fig. 6(c)]. With increasing T_{dep} , both peaks shift away from the H transport sites toward higher energies

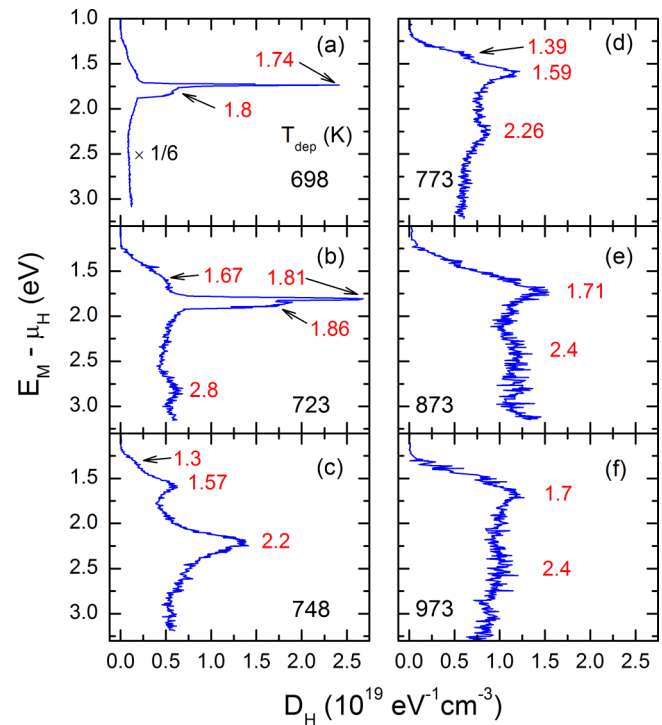


FIG. 6. Hydrogen density-of-states distribution of PLD grown β -Ga₂O₃ thin films as a function of the H chemical potential, $E_M - \mu_H$. The data were derived from the effusion spectra shown in Fig. 3 by applying Eq. (4). The positions of the peaks are indicated in the figure. Note that the plot in (a) is divided by a factor of 6. T_{dep} denotes the deposition temperature.

and ultimately they approach values of $E_M - \mu_H = 1.7$ and 2.4 eV for samples grown at $T_{\text{dep}} \geq 873$ K, respectively [see Figs. 6(d)–6(f)].

To date, little is known about hydrogen related complexes in $\beta\text{-Ga}_2\text{O}_3$ and an assignment of the observed peaks in the H density-of-states to specific hydrogen related complexes is difficult. Recently, predominant H centers such as O–H in a Ga vacancy, Mg–H, and iridium hydrogen complexes were identified and microscopic structures were suggested.^{5–9,19} However, an assignment of the observed peaks in Fig. 6 to specific complexes requires additional information such as the corresponding H binding energies. On the other hand, from the shape and energetic position of the peaks, valuable hints and conclusions regarding potential microscopic structures can be deduced.

Previously, needle-like peaks similar to the data shown in Figs. 6(a) and 6(b) were observed for hydrogen desorption from a polycrystalline tungsten surface.²⁰ This resemblance implies that the narrow peaks observed in the H density-of-states of $\beta\text{-Ga}_2\text{O}_3$ could have a similar origin. However, H desorption from the sample surface as origin for the peaks located at $E_M - \mu_H = 1.74$ and 1.81 eV [Figs. 6(a) and 6(b)] is unlikely since the only difference for the growth of the $\beta\text{-Ga}_2\text{O}_3$ samples is the deposition temperature. If the needle-like peaks were due to pure surface desorption of hydrogen, they should appear in all samples since desorption at the surface would be the rate limiting step.

Another possible origin for the needle-like peaks could be related to the microstructure of the specimens. All $\beta\text{-Ga}_2\text{O}_3$ samples are composed of small grains and grain boundaries. The interface between grains can be regarded as a large internal surface-like structure. Hence, it is conceivable that H accommodated at the grain boundaries could give rise to the needle-like peaks in the H density-of-states distribution. Since all samples are composed of crystalline grains and grain boundaries, the needle-like peak should be observable in all $\beta\text{-Ga}_2\text{O}_3$ samples. This, however, is not the case. Consequently, our data suggest that low growth temperatures favor the formation of large coordination defects in the $\beta\text{-Ga}_2\text{O}_3$ lattice that act as a sink for hydrogen. For silicon and gallium-arsenide, such coordination defects have been reported previously and are well-known as platelets^{21–25} that resemble Guinier–Preston zones²⁶ in metal alloys. In semiconductors, platelets can be generated by hydrogen plasma exposures. For silicon, the nucleation and growth has been investigated thoroughly. Nucleation occurs at low temperatures ($T < 250$ °C), while existing platelets grow in size at higher temperatures where nucleation is suppressed.²⁷ A similar temperature dependence is observed for the needle-like peak in the H density-of-states in $\beta\text{-Ga}_2\text{O}_3$ (see Fig. 6). Hence, based on our data and taking into account the similarity of the behavior of H in other semiconductors, it is conceivable that hydrogen stabilized platelets are generated during the growth of $\beta\text{-Ga}_2\text{O}_3$ at low deposition temperatures. When a sample containing such platelets is heated hydrogen bonds with the host lattice are broken and molecular hydrogen is formed. With increasing time and/or temperature, the number of H_2 increases, which leads to a build-up of internal pressure. At excessive pressure, the H molecules are released and migrate to the surface subsequently giving rise to a sharp peak in the effusion spectrum. Such a behavior has been reported for hydrogenated amorphous silicon that was composed of a

void-rich structure.²⁸ However, to clarify the origin of the needle-like peak in $\beta\text{-Ga}_2\text{O}_3$, more work is needed.

At $T_{\text{dep}} \geq 748$ K, the H density-of-states distribution is mainly composed of two distinctive peaks that settle at $E_M - \mu_H = 1.7$ and 2.4 eV (see Fig. 6). This shows that for $T_{\text{dep}} \geq 748$ K, hydrogen in $\beta\text{-Ga}_2\text{O}_3$ is accommodated in complexes with two different binding energies. An assignment of the peaks to specific H complexes is difficult. The most prominent and stable hydrogen complex consists of a relaxed Ga vacancy with two H atoms ($V_{\text{Ga}}\text{-2H}$) that is aligned along the [102] crystallographic direction.⁶ Often this, H complex is not observed in infrared absorption spectra directly after hydrogenation. However, a low temperature anneal of a hydrogenated samples causes the formation of the $V_{\text{Ga}}\text{-2H}$ complex by activating “hidden” hydrogen.^{5,19} Hidden hydrogen comprises low-energy H complexes such as interstitial H or substitutional H on oxygen sites that dissociate at low temperatures. Subsequently, the mobile H atoms migrate toward Ga vacancies where they can passivate dangling bonds and form $V_{\text{Ga}}\text{-2H}$ complexes. Hence, tentatively, the two peaks observed in the H density-of-states distribution at $E_M - \mu_H = 1.7$ and 2.4 eV can be assigned to hidden hydrogen and $V_{\text{Ga}}\text{-2H}$, respectively.

V. SUMMARY

In summary, hydrogen bonding in $\beta\text{-Ga}_2\text{O}_3$ was investigated by employing H effusion measurements. Significant hydrogen out-diffusion is observed for temperatures above 500 K. Samples deposited at 698 K contain a high H concentration of $8.1 \times 10^{19} \text{ cm}^{-3}$. With increasing T_{dep} , the H concentration decreases to a value of $C_{\text{H}} = 9.2 \times 10^{18} \text{ cm}^{-3}$. From the effusion spectra, the position of the H chemical potential with respect to the H migration states and the H density-of-states were derived. For $\beta\text{-Ga}_2\text{O}_3$ deposited at $T_{\text{dep}} \geq 748$ K, a monotonous increase of the H chemical potential with decreasing H concentration is observed. However, specimens grown at $T_{\text{dep}} = 689$ and 723 K reveal a different behavior. For H concentrations around 10^{19} cm^{-3} , the H chemical potential is pinned at $E_M - \mu_H \approx 1.86$ eV, indicating a high concentration of H sites. This is confirmed by the H density-of-states distribution that revealed a needle-like peak centered around $E_M - \mu_H = 1.74$ and 1.81 eV for $T_{\text{dep}} = 698$ and 723 K, respectively. In addition, both peaks have a shoulder at $E_M - \mu_H = 1.8$ and 1.86 eV. It is likely that the needle-like peaks are caused by large coordination defects that are similar in nature to the well-known Guinier–Preston zones²⁶ in metal alloys. Specimens deposited at higher temperatures show two broad peaks in the H density-of-states distribution that settle at $E_M - \mu_H \approx 1.8$ and 2.4 eV. These peaks are tentatively assigned to hidden hydrogen and $V_{\text{Ga}}\text{-2H}$ complexes.

ACKNOWLEDGMENTS

The authors are grateful to C. Klimm for providing the SEM micrographs.

DATA AVAILABILITY

The data that support the findings of this study are available from the corresponding author upon reasonable request.

REFERENCES

- ¹J. I. Pankove and N. M. Johnson, *Hydrogen in Semiconductors* (Academic Press, San Diego, 1991).
- ²N. H. Nickel, *Hydrogen in Semiconductors II* (Academic Press, San Diego, 1999).
- ³J. B. Varley, J. R. Weber, A. Janotti, and C. G. Van De Walle, *Appl. Phys. Lett.* **97**, 142106 (2010).
- ⁴Y. G. Celebi, R. L. Lichti, B. B. Baker, P. W. Mengyan, H. N. Bani-Salameh, and E. Catak, *Physica B* **407**, 2879 (2012).
- ⁵Y. Qin, M. Stavola, W. B. Fowler, P. Weiser, and S. J. Pearton, *ECS J. Solid State Sci. Technol.* **8**, Q3103 (2019).
- ⁶P. Weiser, M. Stavola, W. B. Fowler, Y. Qin, and S. Pearton, *Appl. Phys. Lett.* **112**, 232104 (2018).
- ⁷N. H. Nickel, F. Lang, E. G. Villora, K. Shimamura, and J. Rappich, *AIP Adv.* **9**, 105026 (2019).
- ⁸J. R. Ritter, K. G. Lynn, and M. D. McCluskey, *J. Appl. Phys.* **126**, 225705 (2019).
- ⁹J. R. Ritter, J. Huso, P. T. Dickens, J. B. Varley, K. G. Lynn, and M. D. McCluskey, *Appl. Phys. Lett.* **113**, 052101 (2018).
- ¹⁰N. H. Nickel, W. B. Jackson, and J. Walker, *Phys. Rev. B* **53**, 7750 (1996).
- ¹¹N. H. Nickel and I. E. Beckers, *Phys. Rev. B* **66**, 075211 (2002).
- ¹²N. Nickel, *Phys. Rev. B* **73**, 195204 (2006).
- ¹³S. Geller, *J. Chem. Phys.* **33**, 676 (1960).
- ¹⁴D. Dohy, G. Lucazeau, and A. Revcolevschi, *J. Solid State Chem.* **45**, 180 (1982).
- ¹⁵J. W. Bozzelli and R. B. Barat, *Plasma Chem. Plasma Process.* **8**, 293 (1983).
- ¹⁶S. Roychowdhury, U. K. Roychowdhury, and M. Venugopalan, *Plasma Chem. Plasma Process.* **2**, 157 (1982).
- ¹⁷N. H. Nickel and K. Geilert, *Appl. Phys. Lett.* **116**, 242102 (2020).
- ¹⁸W. B. Jackson, A. J. Franz, H. C. Jin, J. R. Abelson, and J. L. Gland, *J. Non-Cryst. Solids* **227–230**, 143 (1998).
- ¹⁹N. H. Nickel, F. Lang, E. G. Villora, K. Shimamura, and J. Rappich, *H and D Related Modes in B-Ga₂O₃* (unpublished).
- ²⁰P. A. Redhead, *Vacuum* **12**, 203 (1962).
- ²¹N. M. Johnson, F. A. Ponce, R. A. Street, and R. J. Nemanich, *Phys. Rev. B* **35**, 4166 (1987).
- ²²J. R. Botha, J. H. Neethling, and A. W. R. Leitch, *Semicond. Sci. Technol.* **14**, 1147 (1999).
- ²³N. H. Nickel, G. B. Anderson, N. M. Johnson, and J. Walker, *Phys. Rev. B* **62**, 8012 (2000).
- ²⁴E. V. Lavrov and J. Weber, *Phys. Rev. Lett.* **87**, 185502 (2001).
- ²⁵N. H. Nickel, G. B. Anderson, N. M. Johnson, and J. Walker, *Physica B* **273–274**, 212 (1999).
- ²⁶J. B. Cohen, *Solid State Phys. Adv. Res. Appl.* **39**, 131 (1986).
- ²⁷N. M. Johnson, C. Herring, C. Doland, J. Walker, G. B. Anderson, and F. A. Ponce, *Mater. Sci. Forum* **83–87**, 33 (1992).
- ²⁸S. Jafari, J. Steffens, M. Wendt, B. Terheiden, S. Meyer, and D. Lausch, *Phys. Status Solidi Basic Res.* **257**, 2000097 (2020).